



# Mechanical, electrical and thermal properties of graphene oxide-carbon nanotube/ ABS hybrid polymer nanocomposites

Jeevan Jyoti<sup>1,2</sup> · Abhishek K. Arya<sup>1</sup> · Sreekumar Chockalingam<sup>1</sup> · Shailesh K. Yadav<sup>1</sup> · Kiran M. Subhedar<sup>1</sup> · S. R. Dhakate<sup>1</sup> · Bhanu Pratap Singh<sup>1,2</sup>

Received: 6 February 2020 / Accepted: 11 August 2020 / Published online: 24 August 2020  
© The Polymer Society, Taipei 2020

## Abstract

Multiwalled carbon nanotubes (MWCNTs), functionalized carbon nanotubes (FCNTs) and graphene oxide-carbon nanotube (GCNTs) hybrid Bucky paper (BP) reinforced acrylonitrile-butadiene-styrene (ABS) composites are prepared via vacuum filtration followed by hot compression molding. The nanomechanical, electrical and thermal properties of these BP reinforced ABS composites are studied. The nanoindentation hardness and elastic modulus of GCNTs-ABS hybrid composites reached to  $389.98 \pm 91.79$  MPa and  $7669.6 \pm 1179.12$  MPa respectively. Other nanomechanical parameters such as plastic index parameter, elastic recovery, the ratio of residual displacement after load removal and displacement at maximum load are also investigated. The improved nanomechanical properties are correlated with Raman spectroscopy and scanning electron microscopy (SEM). It is found that GCNTs and their composites showed the higher value of defect density. The maximum value of defect density range for GCNTs and GCNTs-ABS is (297.4 to 159.6) and (16.0 to 1.6), respectively. The higher defect density of GCNTs indicates that the interfacial interaction between the ABS, which was further correlated with electrical and thermal properties. Additionally, the through-plane electrical conductivities of MWCNTs, FCNTs and GCNTs based ABS composites were  $6.5 \pm 0.6$ ,  $4.5 \pm 0.7$  and  $6.97 \pm 1.2$  S/cm respectively and thermal conductivities of MWCNTs, FCNTs and GCNTs reinforced ABS composites; 1.80, 1.70 and 1.98 W/mK respectively. These GCNTs-ABS composites with this value of thermal conductivity can be used in various applications of efficient heat dissipative materials for electronic devices.

**Keywords** Bucky paper · Multiwalled carbon nanotube (MWCNTs) · Functionalized carbon nanotube (FCNTs) · Graphene oxide-carbon nanotube (GCNTs)

## Introduction

In the past few years, reinforcement of nanofillers in polymer composites has been drawing much more attention due to their extraordinary properties. The nanofiller-reinforcement enhances the mechanical, electrical and thermal properties of polymer composites. Incorporation of different type of carbon

nanomaterials such as carbon nanofiber, carbon nanotubes (CNTs), graphene, graphene oxide (GO) and reduced graphene oxide (RGO) has shown potential to improve the mechanical properties of polymer matrices [1–6]. Among all the carbon-based nanomaterials, CNTs show the excellent combination of properties like strength and Young's modulus [7–10]. Multiwalled carbon nanotubes (MWCNTs) have been widely utilized as the reinforcing filler for high strength polymer composites [11–16]. Previous studies on MWCNTs based polymer composites showed that the utilization of MWCNTs in composites strongly depend upon uniform dispersion of CNTs throughout the polymer matrix [17–19]. The enhancements in properties of polymer composites are strongly dependent upon filler-matrix interaction. However, CNTs suffer the problem of poor dispersion due to van der Waals force of attraction arises as a result of  $\pi$ - $\pi$  interactions along their axis [20–22].

Graphene, a two-dimensional carbon material, is known as the thinnest material which is one atom thick  $sp^2$  layer of

**Electronic supplementary material** The online version of this article (<https://doi.org/10.1007/s10965-020-02252-9>) contains supplementary material, which is available to authorized users.

✉ Bhanu Pratap Singh  
bps@nplindia.org; bpsingh2k4@yahoo.com

<sup>1</sup> Advanced Carbon Products and Metrology, Advanced Materials and Devices Metrology, CSIR-National Physical Laboratory, Dr. K.S. Krishnan Marg, New Delhi, India

<sup>2</sup> AcSIR-National Physical Laboratory, New Delhi 110012, India

hybridized carbon atoms. Graphene has excellent structural, mechanical, thermal, electrical and optical properties which have attracted extensive interest in the field of research [23–28]. Due to these superior features graphene and graphene-like nanomaterials have been used in many applications like polymer nanocomposites [29], supercapacitors [30, 31], nanoelectronics [32], energy storage devices [33], batteries [34] and sensors. However, the main drawbacks of using graphene are their restacking. To avoid these problems, i.e. agglomerations in CNTs and restacking in graphene, a hybrid material of graphene oxide and CNTs have been synthesized by implementing various previously reported techniques [35–38].

Agglomeration and interfacial restacking problems are expected to overcome by using the hybrid nanofillers in polymer nanocomposites, simultaneously. Currently, most commonly used nanofillers for polymer composites are one dimensional (1D) single-walled and multiwall carbon nanotubes, two-dimensional (2D) graphene oxide and reduced graphene oxide. The hybridization of 1D CNTs and 2D graphene oxide flakes lead to the 3D hybrid nanomaterials (GCNTs), which possess excellent performance and properties of individual nanomaterial [39].

In previous literature, polymer-hybrid nanocomposites had shown the extraordinary mechanical and energy absorbing properties [40–45]. Graphene and CNTs hybrid was found to be quickly dispersed in water [46]. Shin et al. [47] studied the toughness properties of composite fibers prepared by the self-alignment of reduced graphene oxide-MWCNTs (GCNTs). The result represents that the toughness was increased by the addition of GCNTs flakes in solution spun polymer fibers. The value of toughness was increased due to the interconnected network structure between GCNTs. Chatterjee et al. [48] studied the mechanical properties of graphene nanoplatelets and CNTs hybrid epoxy composites prepared by the in-situ polymerization. The CNTs-graphene nanoplatelets ratio (9:1) represents the remarkable improvement in fracture toughness (increased up to 76%). Gong et al. [49] studied the synergetic effect of reduced graphene oxide (RGO)-double walled carbon nanotube (DWCNTs) on the toughness of polymer nanocomposites. The tensile strength and toughness of RGO-DWCNTs nanocomposites reached to  $374.1 \pm 22.8$  MPa and  $9.2 \pm 0.8$  MJ/m<sup>3</sup> respectively. Kim et al. [50] studied the enhancement in mechanical properties of MWCNTs-Et-GO/LLDPE (linear low-density polyethylene) composites. This structure represents the attachment of MWCNTs with GO and ethylene diamine (Et-GO). The tensile strength of Et-GO-MWCNTs/LLDPE composite with 1% loading enhanced up to 147.8% as compared to pure LLDPE. Yingkui Yang et al. [51] studied the nanomechanical and thermal properties of covalently-functionalized graphene polymer composites. Functionalized graphene (FG) was obtained by grafting m-isopropenyl- $\alpha$ ,  $\alpha'$ -dimethyl benzyl

isocyanate (m-TMI) to graphene oxide (GO) followed by the chemical and solvothermal reduction of GO. The FG sheets were formed, which were hydrophobic in nature and stable in polar solvents such as N, N dimethylformamide. The vinylbenzyl groups of m-TMI were attached to FG copolymerized with methyl methacrylate to produce graphene/poly (methyl methacrylate) (PMMA) composites. Well-dispersed FG sheet in PMMA formed strong interfacial bonds with the matrix, contributing to increases in elastic modulus (i.e. 72.9%) and indentation hardness (i.e. 51.2%) on the addition of at 1% wt FG sheet. Fan et al. [52] studied the nanomechanical properties of graphene nanosheet (GNS)/hydroxyapatite (HA) nanorod composites (GNS/HA). The mechanical properties of HA and GNS/HA coatings deposited on the glass slides by spin coating were examined using nanoindentation technology on a TI-950 tribo indenter system. The value of hardness and Young's modulus was found to be  $242.06 \pm 7.28$  MPa and  $6.20 \pm 1.67$  GPa, respectively in GNS/HA nanorod composite.

Herein, we report the electrical, thermal and nanomechanical properties of MWCNTs, FCNTs and GCNTs reinforced ABS polymer nanocomposites prepared by vacuum filtration followed by hot compression molding to avoid the agglomeration problem in CNTs. The three dimensional (3D) network structure of GCNTs hybrid were studied by scanning electron microscope (SEM). Raman spectroscopic analysis was carried out to correlate the morphological and physical properties with nanomechanical properties of carbon nanofiller based ABS composites. The nanomechanical, electrical and thermal conductivity of GCNTs, MWCNTs and FCNTs filled ABS composites were studied and a synergistic effect is investigated.

## Materials

ABS is a tri-polymer of acrylonitrile, butadiene, and styrene (density- $1.068$  g/cm<sup>3</sup> and melt flow index (MFI)  $100$  °C/10 kg) which was obtained from Bhansali group (India). MWCNTs were synthesized using toluene (C<sub>7</sub>H<sub>8</sub>, 99% pure) as a hydrocarbon source and ferrocene ((C<sub>10</sub>H<sub>10</sub>) Fe, 99%) as a catalyst precursor in an in-house built CVD set up [53]. N-N dimethylformamide (DMF) (C<sub>3</sub>H<sub>7</sub>NO, 99%), nitric acid (HNO<sub>3</sub>, 65%), and acetone (C<sub>3</sub>H<sub>6</sub>O, 99.9%) were obtained from Sigma Aldrich and used without further purification.

## Synthesis of acid functionalized MWCNTs, FCNTs and GCNTs hybrid

First, MWCNTs were synthesized by CVD method in which toluene was used as hydrocarbon source and ferrocene as a catalyst. The diameter of MWCNTs was in the range of 10–100 nm. The average diameter of CNTs was approximate 25.8 nm and the average bundle length 350  $\mu$ m [54]. As

produced MWCNTs were treated with the nitric acid ( $\text{HNO}_3$ , 60% conc.) for 24 h in the refluxing apparatus at 70 °C, to attach carboxylic (COOH) group on the MWCNTs surface [55]. These acid functionalized CNTs were washed repeatedly with DI water to reach neutral pH and thereafter dried in the oven at 100 °C for 12 h. These acid functionalized CNTs were designated as FCNTs.

Second, graphene oxide was synthesized by improved Hummer method [56]. GO-CNTs (GCNTs) hybrid was synthesized using the ultra-sonication technique and produced GO and CNTs were added to ethanol solution in 1:1 ratio and ultrasonicated for 8 h and discussed elsewhere [18]. The final sample was denoted as GCNTs hybrid.

### Preparation of MWCNTs, FCNTs and GCNTs bucky papers

Buckypaper (BP) is a freestanding thin porous network of randomly entangled CNTs cohesively bound by van der Waals's force of interactions. BPs were prepared from MWCNTs, FCNTs and GCNTs nanofillers individually. These three different carbon nanofillers were separately dispersed in a solvent medium and subsequent vacuum filtered through filter paper.

As shown in Fig. 1 for the synthesis of BP of MWCNTs, FCNTs, and GCNTs, these were separately suspended in the acetone and sonicated in an ultrasonic bath for 3 h. Further, the suspended material was filtered with vacuum filtration technique by applying an adequate pressure. Later, samples were dried in an oven at 70 °C for overnight. The thickness of all BPs was in the range of 90–100  $\mu\text{m}$ . Before characterization, ABS and the BPs were placed in an oven at 100 °C for 24 h to

remove absorbed moisture as well as solvent. The concentration of carbon filler and ABS are 60:40%.

### Preparation of carbon nanomaterials based bucky paper reinforced ABS composites

ABS granules were dissolved in 50 ml of DMF solution using magnetic stirrer for 6 h. After complete dissolution of ABS granules, it was coated on both sides of BPs.

This consolidation cycle is optimization for minimizing the internal porosity and improving the impregnation of the polymer in BPs. As prepared BP-ABS composite papers were cut into small specimens according to the mold's dimension (50 mm $\times$ 50 mm) for composite preparation as shown in Fig. 2. After cutting, these were stacked into the mold and pressure was applied of 100 kg/cm<sup>2</sup> using the hydraulic press at temperature 265 °C, the sample was cooled down at the room temperature slowly.

### Characterizations

Surface morphology of different MWCNTs-ABS, FCNTs-ABS and GCNTs-ABS based BP composites were examined by Scanning Electron Microscope (SEM, model EVO-MA10 ZEISS). Raman spectra of the composite samples were obtained using in-via Raman spectrometer, UK, using the two excitation of laser source of 785 nm (1.58 eV) and 514 nm (2.34 eV) wavelengths and Raman spectrum was recorded by scanning in 500 to 3200  $\text{cm}^{-1}$  region. The nano-indentation study was carried out by IBIS-Nano-indentation

**Fig. 1** Schematic diagram of the preparation of Bucky paper (MWCNTs, FCNTs, and GCNTs)

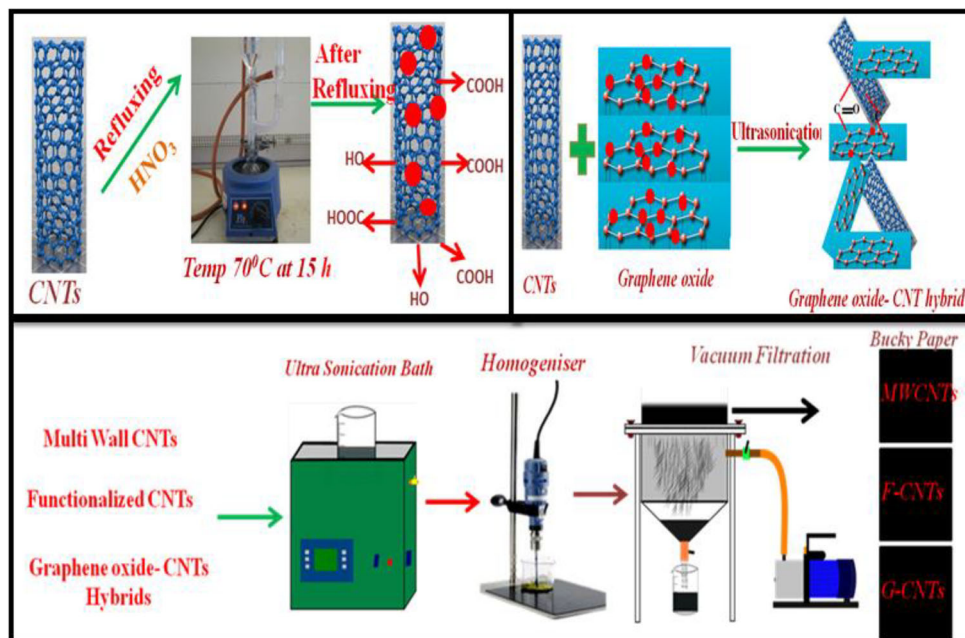
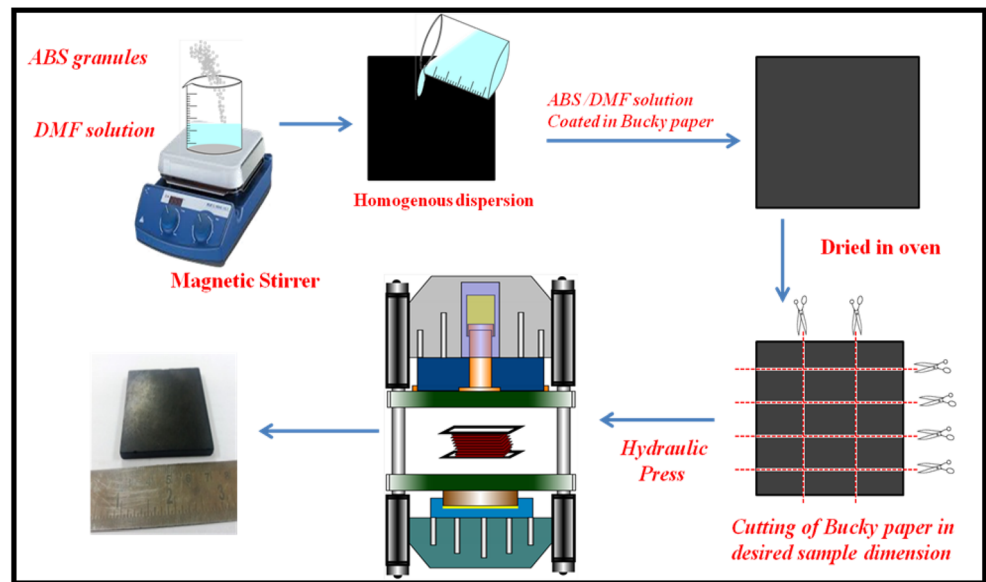


**Fig. 2** Systematic diagram for the formation of MWCNTs-ABS, FCNTs-ABS and GCNTs-ABS composite samples



systems equipped with a Berkovich indenter, and other details are given elsewhere [57].

Electrical conductivity of the composites was measured by the four-point probe technique (Keithley 224 programmable current source). The voltage drop (V) between the two points of distance 1.5 cm was measured by Keithley 197 A and by auto ranging microvolt digital multimeter. The densities of the samples were measured by conventional Archimedes's principle and found to very close to its theoretical value. Thermal diffusivity measurement was carried out by laser flash system Linseis (LFA 1023) on the polished samples of the disc, dimension 12.75 mm diameter and thickness 2.25 mm. Specific heat measurement was performed by differential scanning calorimeter (204 F1 pheonix). The thermal conductivity was calculated from the equation.

$$\alpha = \frac{\kappa}{\rho C_p} \quad (1)$$

where  $\alpha$  is the thermal diffusivity,  $\kappa$  is the thermal conductivity,  $C_p$  is the specific heat and  $\rho$  is the density.

## Results and discussion

### Mechanical properties by nanoindentation

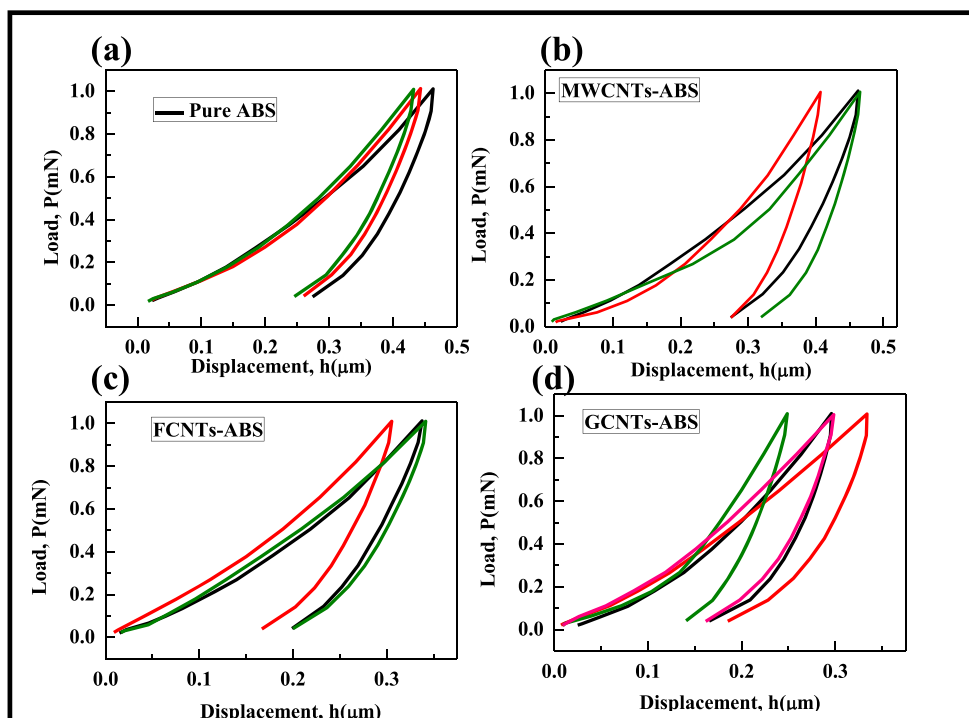
Nanoindentation is an important technique to study the mechanical properties of polymer composites. The nanomechanical testing provides information about various mechanical properties such as hardness (H), elastic modulus (E), load displacement curve, elastic recovery, etc. The load displacement curves for ABS, MWCNTs-ABS, FCNTs-ABS and

GCNTs-ABS at minimum indentation load of 1mN are studied and shown in Fig. 3a-d.

Load versus displacement curves are used to investigate the elastic and plastic properties of polymer composites. Elastic modulus and hardness is a function of slope for unloading curve in nanoindentation measurements (Fig. 3). Figure 3a shows that maximum displacement is an indicator of the soft matrix that consequently leads to the low Young's modulus. The GCNTs-ABS had the least displacement that is attributed to the highest Young's modulus under the same indentation conditions similar for others. It is because of lower displacement signifies the strengthening of the matrix in presence of different carbon nanofillers [58]. In the current study, the curve shifts toward the left and lower displacements as a result of matrix strengthening as previously discussed by Ostovan et al. [59].

It is depicted in Fig. 4a that the value of H for pure ABS, MWCNT-ABS, FCNTs-ABS, and GCNTs-ABS is  $248.59 \pm 26.32$  MPa,  $306.32 \pm 26.74$  MPa,  $341.10 \pm 40.09$  MPa, and  $389.98 \pm 91.79$  MPa, respectively. A similar trend is been observed in Fig. 4b for elastic modulus property of the samples; ABS, MWCNT-ABS, FCNTs-ABS and GCNT-ABS composites and the values are  $4505.72 \pm 261.96$  MPa,  $6096.99 \pm 185.96$  MPa,  $6600.18 \pm 1184.45$  MPa and  $7669.61 \pm 1179.12$  MPa, respectively. Thus, an overall improvement in elastic modulus is 35.32% for MWCNTs-ABS, 46.49% for FCNTs-ABS, 70.22% for GCNTs-ABS and similarly the overall improvement in hardness is 23.02% for MWCNTs-ABS, 36.99% for FCNTs-ABS and 56.62% for GCNTs-ABS in reference with pure ABS polymer. In addition to elastic modulus and hardness properties, the wear resistance is also an important parameter in determining the behavior of polymer composites.

**Fig. 3** Load versus displacement curves of (a) ABS, (b) MWCNTs-ABS, (c) FCNTs-ABS and (d) GCNTs-ABS composites

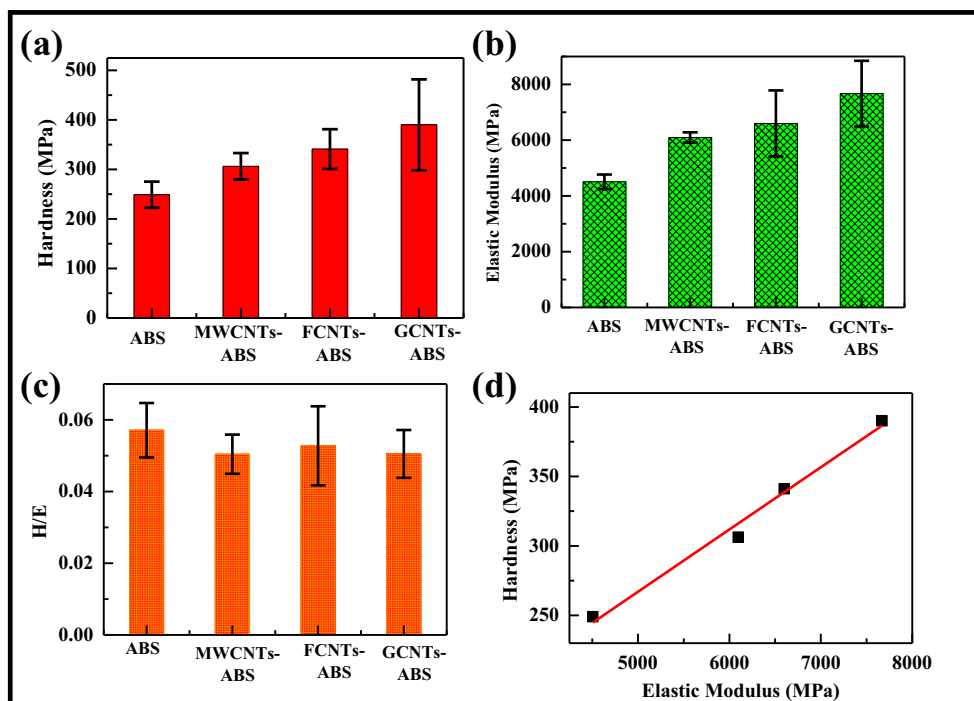


The lower value of H/E in MWCNTs-ABS composite signifies that the fraction of work is being consumed in plastic deformation. On the other hand, the value of H/E in GCNTs-ABS composite (0.051) indicate less plastic deformation as compared to pure ABS and FCNTs-ABS composites. The H versus E curve of all carbon nanofiller

reinforced ABS composites is shown in Fig. 4d. The H and E follow linear behavior point towards the toughness of the structure.

Load versus displacement curves are used to calculate the  $h_{res}/h_{max}$ , elastic recovery (ER) and the stiffness. The value of ER is calculated by using the relation

**Fig. 4** Variation of (a) hardness, (b) elastic modulus, (c) (H/E) at 1mN indentation load and (d) linear behavior of the H-E curve of different type of carbon nanofiller reinforced ABS composites



$$\%ER = \frac{h_{\max} - h_{\text{res}}}{h_{\max}} \times 100 \quad (2)$$

Where,  $h_{\max}$  is the maximum displacement of load and  $h_{\text{res}}$  is the residual displacement after removing load. The ratio of  $h_{\text{res}}/h_{\max}$  curves of various polymer composites are shown in Fig. 5a. A value of this parameter varies from 0.52–0.62 which corresponds to the elastic and plastic behavior. The lesser limits are resultant of the elastic behavior, and upper limit corresponds to rigid plastic behavior. Elastic recovery of material depends upon the elastic behavior of material. In this work value of ER for different carbon nanofiller reinforced ABS composites vary in the range of 38.5–49.42% (Fig. 5b). The estimation of contact stiffness  $(dp/dh)_{\max}$  has been verified with the elastic and plastic properties of the polymer. Stiffness is defined as the resistance of an elastic body to deformation under the load. The variations in the stiffness of composite samples are shown in Fig. 5c. The value of the stiffness for pure ABS polymer is  $5.2 \pm 0.08 \times 10^3 \text{ N m}^{-1}$  which increased for GCNTs-ABS composite sample up to  $7.65 \pm 1.22 \times 10^3 \text{ N m}^{-1}$ .

The deformation energy ( $U_r$ ) of different carbon nanofillers (MWCNTs, FCNTs, GCNTs reinforced ABS) composites is shown in Fig. 5d. Generally,  $U_r$  of the polymer composites is estimated by the area that is surrounded by loading–unloading curve in the load-displacement profile. Here in this work, deformation energy is calculated by the relation given in Eq. (3) [60, 61].

$$U_r = \left( \frac{1}{3} \sqrt{\frac{1}{\omega_0 \tan^2 \varphi}} \right) \frac{1}{\sqrt{H}} P^3/2 \quad (3)$$

Where  $\omega_0$  is the geometry constant, and it has the value of 1.3 for the pyramidal indenter,  $P$  is the load and  $\varphi$  is the half angle of the Berkovich Indenter and has a value of  $65.3^\circ$ . The variation in deformation energy with different carbon nanofillers (MWCNTs, FCNTs, and GCNTs) loading in ABS is shown in Fig. 5d. The values of  $U_r$  are found to be in the range of  $1.50 \pm 0.08 \times 10^{-10}$  to  $1.19 \pm 0.17 \times 10^{-10} \text{ J}$ . The value of  $H$  and  $U_r$  strongly depended upon the ER. The results for  $U_r$  are also in good agreement with results for  $H$ . The GCNTs-ABS composites possess excellent mechanical properties which are further correlated with the Raman study. The Raman analysis technique was used to determine the value of defect density and defect density generated the interfacial bonding.

### Raman spectroscopic analysis

Carbon nanofillers and their reinforced ABS composites are characterized using Raman spectroscopy at two laser excitation energy. To obtain information about the interaction between carbon nanofiller and ABS matrix as shown in Fig. 6. Raman spectra of carbon nanofillers reinforced ABS composite showed three characteristics peaks: First-D band ( $1304\text{--}1350 \text{ cm}^{-1}$ ) attributed to the defects in nanofillers including  $sp^3$  hybridized, second- an intense G band ( $1480\text{--}1581 \text{ cm}^{-1}$ ) associated with tangential C-C bond stretching motion and the

**Fig. 5** Variation of (a)  $h_{\text{res}}/h_{\max}$ , (b) elastic recovery %, (c) stiffness and (d) deformation energy of carbon nanofiller reinforced ABS composites at 1mN indentation loading

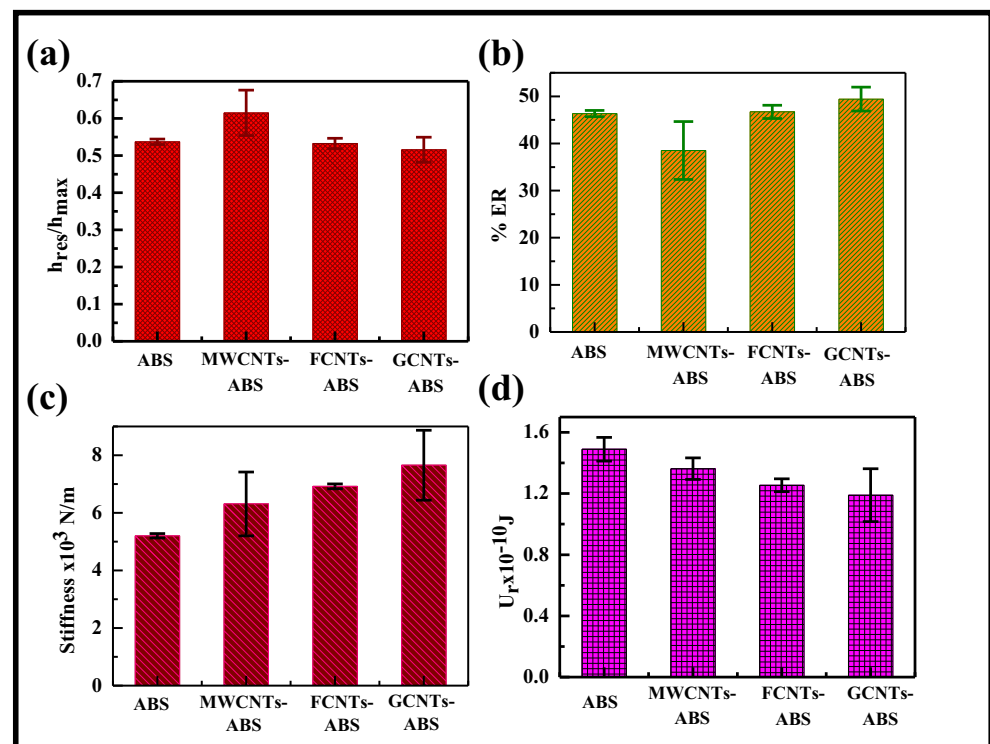
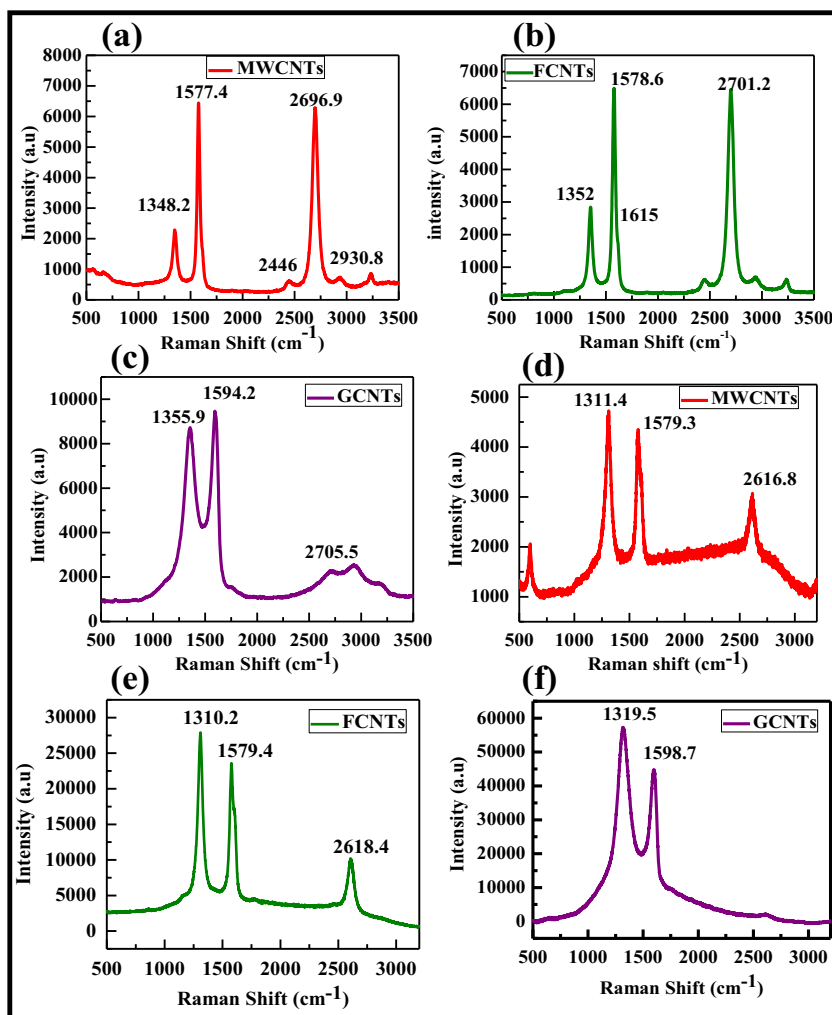


**Fig. 6** Raman spectra of (a) MWCNTs, (b) FCNTs, (c) GCNTs at the laser excitation wavelength 514 nm, (d) MWCNTs (e) FCNTs, and (f) GCNTs at the laser excitation wavelength 785 nm



last 2D band (2600-2700 cm<sup>-1</sup>) which is overtone of D band [62–64]. Raman Spectra of pure ABS as shown in Figure P3 (given in Supplementary information).

Raman spectroscopy can discriminate defects related to the size in sp<sup>2</sup> carbon lattices, resulting in different intensity ratio depending on the amount of disorder. The amount of disorder in a nano-crystallite is given by the amount of border (one dimensional defect) on the total crystalline area, and this is a measurement of the nano-crystallite size L<sub>a</sub>. Point-like defects, distance between defects L<sub>D</sub> measures of the amount of disorder, and recent experiment showed that different approaches must be used to quantify L<sub>D</sub> and L<sub>a</sub> by Raman spectroscopy (See in schematic diagram of supplementary information P1 (MWCNTs) and P2(GCNTs)) [65].

This Raman study mainly focuses on the low distance defect density regime (L<sub>D</sub> ≥ 10 nm). The total area contributing to the D band scattering is proportional to the point defects, giving rise to the I<sub>D</sub>/I<sub>G</sub> ∝ 1/L<sub>D</sub><sup>2</sup>. The ratio between G and D bands depended upon the fourth power of the laser excitation energy. The value of L<sub>D</sub> is calculated in term of the energy using the following equation [66].

$$L_D^2 \text{ (nm}^2\text{)} = \frac{(4.3 \pm 1.3) \times 10^3}{(E_L^4)} \left(\frac{I_D}{I_G}\right)^{-1} \quad (4)$$

Regarding the excitation laser wavelength λ<sub>L</sub> (in nanometers), it can be represented as

$$L_D^2 \text{ (nm}^2\text{)} = (1.8 \pm 0.5) \times 10^{-9} \lambda_L^4 \left(\frac{I_D}{I_G}\right)^{-1} \quad (5)$$

The Eq. (4) and (5) are an empirical formula which is used to quantify the amount of point like a defect in the carbon material using laser excitation energy/wavelength. In term of the defect density n<sub>D</sub>(cm<sup>-2</sup>) = 10<sup>14</sup>/(πL<sub>D</sub><sup>2</sup>), the Eqs. (4) and (5) become [66].

$$n_D \text{ (cm}^{-2}\text{)} = (7.3 \pm 2.2) \times 10^9 E_L^4 \left(\frac{I_D}{I_G}\right) \quad (6)$$

$$n_D \text{ (cm}^{-2}\text{)} = \frac{(1.8 \pm 0.5) \times 10^{22}}{\lambda_L^4} \frac{(I_D)}{(I_G)} \quad (7)$$

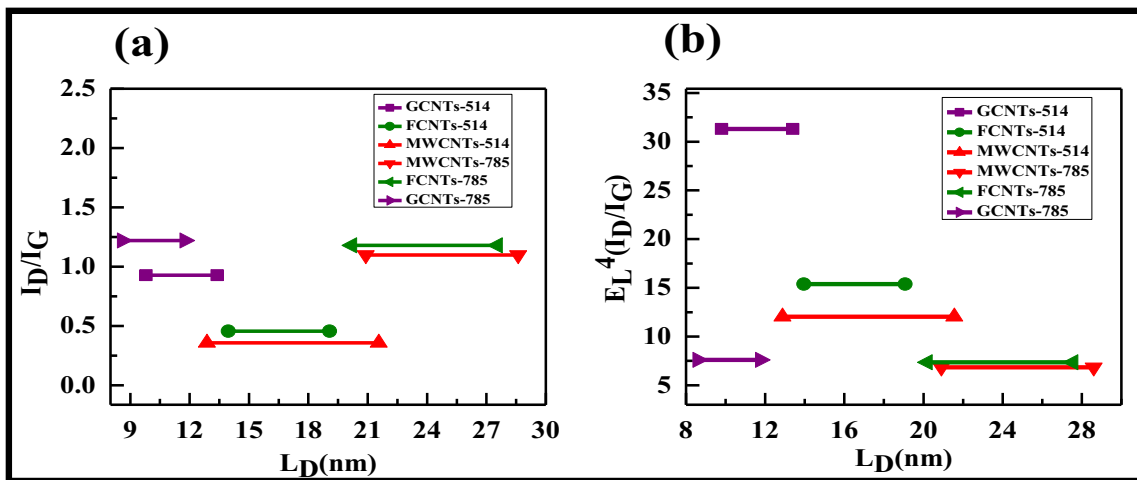


Fig. 7 Variations of (a)  $I_D/I_G$  as function of  $L_D$  for different carbon nanofiller and laser excitation energy and (b)  $E_L^4(I_D/I_G)$  as a function of  $L_D$

Figure 6 shows the Raman spectrum of different carbon nanofillers with different laser wavelength. Figure 7 plot, shows that the intensity ratio of D and G band depends upon the excitation energy and quality of the carbon material. In Fig. 7 different laser excitation energy is used, and the value of  $I_D/I_G$  increases as  $L_D$  decreases (See supplementary information Table S1). The value of  $L_D$  gives important information to understand the defect peak.

The value of  $L_D$  is large in case of MWCNTs as compared to others because MWCNTs have high quality (See in supplementary information S1). The value of defect density was calculated by Eq. (6).

Figure 8 shows the calculated defect density between the different carbons based nanofiller. Defect density present in MWCNTs has a smaller value as compared to the other. While, GCNTs hybrid has high ordered defect density due to the carbonyl groups which are present in GO. Further, the

higher value of  $L_D$  shows the smaller defect density value and turns out to have a highvalue of crystallite size.

The general expression that gives crystallite size ( $L_a$ ) from the integrated intensity ratio  $I_D/I_G$  using a laser is given by Eq. (8). To calculate the value of nano-crystallite size different laser energies of different excitation were used. Further,  $L_a$  derived from the following equation in terms of energy [67].

$$L_a \text{ (nm)} = \frac{560}{E_L^4} \left( \frac{I_D}{I_G} \right)^{-1} \tag{8}$$

In term of the wavelength, the Eq. (8) becomes [67].

$$L_a \text{ (nm)} = (2.4 \times 10^{-10}) \lambda_L^4 \left( \frac{I_D}{I_G} \right)^{-1} \tag{9}$$

Integrated intensities ratio of the D and G bands ( $I_D/I_G$ ) vs  $L_a$  for all samples and laser energies used in the

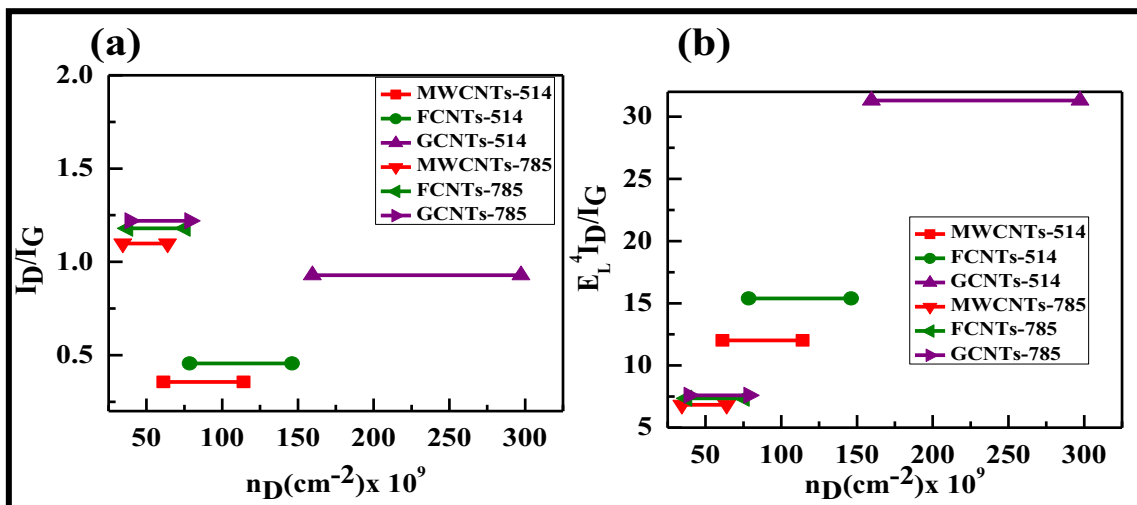
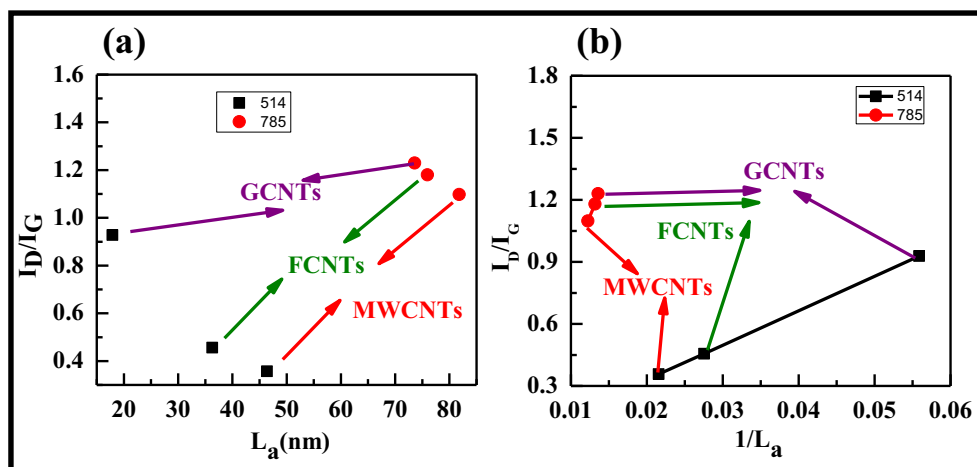


Fig. 8 Variations of (a)  $I_D/I_G$  as function of defect density ( $n_D$ ) for different carbon nanofiller and laser excitation energy and (b)  $E_L^4(I_D/I_G)$  as a function of  $n_D$  according to Eqs. 6

**Fig. 9** Variations of (a)  $I_D/I_G$  as function of  $L_a$  (nm) of nanofiller and laser excitation energy and (b) ( $I_D/I_G$ ) as a function of  $1/L_a$  ( $\text{nm}^{-1}$ ) according to Eqs. 8



experiment. The value of intensity ratio of  $I_D/I_G$  was increased the value of  $L_a$  goes on decreasing. Figure 9b shows the straight line, its represents the experimental value of intensity ratio of D and G band versus crystallite size ( $1/L_a$ ).

In GCNTs-ABS, FCNTs-ABS composites, the peak positions slightly shifted and intensity decreased as compared to the MWCNTs-ABS composites, which is being confirmed by Fig. 10 at two laser wavelength (785 and 514 nm). The shifting of Raman peaks towards lower or higher wave

**Fig. 10** Raman spectra of (a) MWCNTs-ABS (b) FCNTs-ABS, (c) GCNTs-ABS at the laser excitation wavelength 514 nm, (d) MWCNTs-ABS (e) FCNTs-ABS, and (f) GCNTs-ABS at the laser excitation wavelength 785 nm

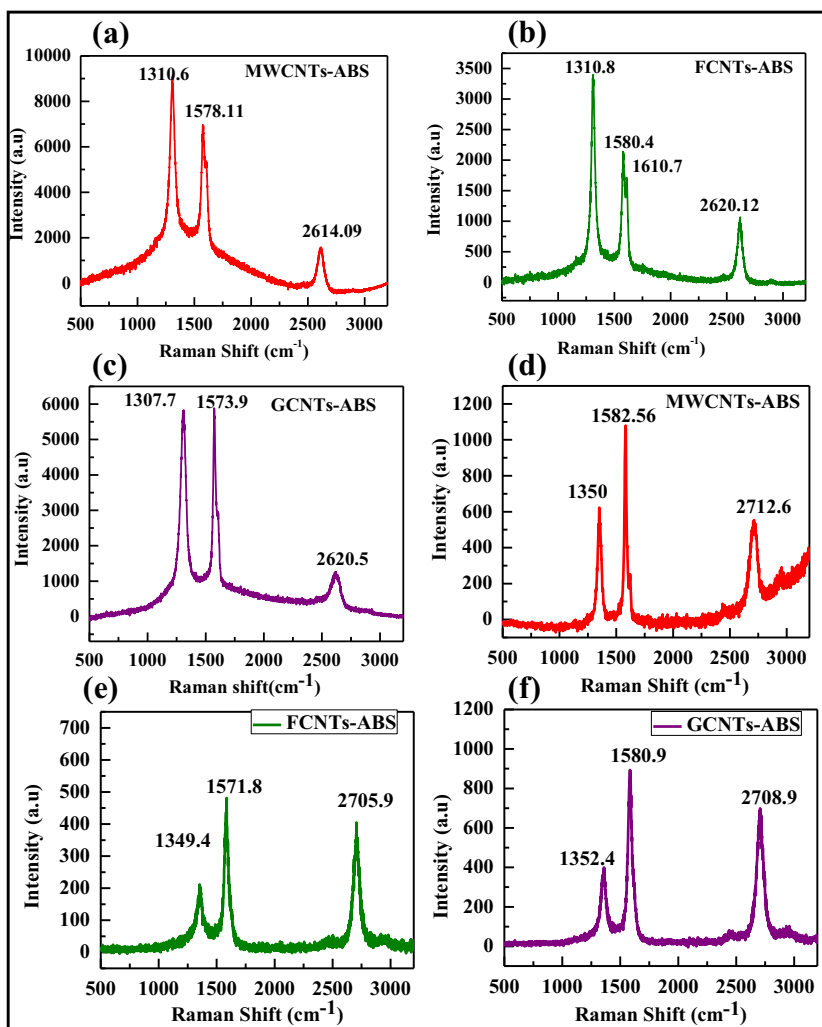
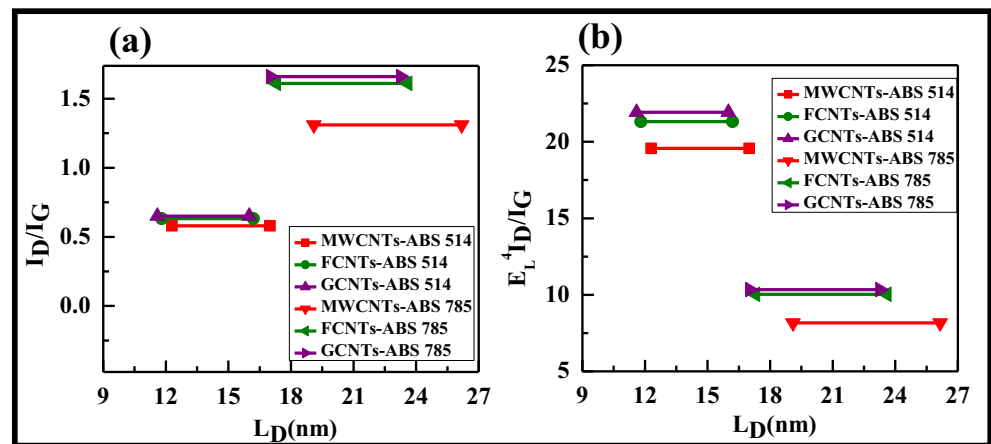


**Fig. 11** Variations of (a)  $I_D/I_G$  as function of  $L_D$  for different carbon-based nanofiller reinforced ABS composites and laser excitation energy and (b)  $E_L^4 (I_D/I_G)$  as a function of  $L_D$  according to Eqs. 4



number is related to the chemical bond length of molecules. Shorter bond length causes a shift towards higher wavenumber or vice versa. If the chemical bond length of molecules changes due to any internal or external effects, then it may cause a shift in wavenumber.

The plot in Fig. 11 validates these relations for samples with  $L_D > 10$  nm. The value of  $L_D$  of MWCNTs-ABS is enhanced higher than other two materials.

Figure 12 shows the density of the defects in different carbon-based nano-fillers. GCNTs have a smaller value as compared to the other. GCNTs incorporated composites have high ordered defect density due to the GO, and they shape the bonding between the ABS matrix as compare to the FCNTs-ABS and MWCNTs-ABS composites (See supplementary information Table S2).

Figure 13a shows the plot of the intensities ratio of the D and G bands ( $I_D/I_G$ ) vs  $L_a$  for all carbon nanofillers reinforced ABS composites and laser energies used. Different points are observed with increasing the value of  $L_a$ . Figure 13b shows that all experimental points collapse in the decreasing the value of the  $I_D/I_G$  vs  $1/L_a$  plot. The value of MWCNTs-ABS is larger as compared to other because of crystallization nature as

compared to other (See supplementary information Table S2).

### Morphological characterization of bucky paper -ABS nano composites

To observe the impregnation of ABS polymer in these composites, their surface morphology was examined using SEM. SEM images of carbon-based ABS composites are shown in Fig. 14. Different morphologies were observed in different types of CNT BP. By applying the hydraulic pressure on the sample papers of BP- ABS, ABS matrix was forced to penetrate into the bucky paper, but due to its low permeability, resin displaced into the chains and generates random channels through the nanotube network.

To observe the impregnation quantity of the manufactured composites, their surface morphology of carbon nanofiller BP-ABS composites are shown in Fig. 14. The MWCNTs-ABS BP composites exhibited the minimum porosity and high degree of the resin impregnation as shown in Fig. 14a and b. FCNTs-ABS composites prepared by hot compression are quite heterogenous, showing the matrix rich region and non impregnation area in Fig. 14c and d. The good impregnation

**Fig. 12** Variations of (a)  $I_D/I_G$  as function of defect density ( $n_D$ ) for different carbon-based nanofiller reinforced ABS composites and laser excitation energy and (b)  $E_L^4 (I_D/I_G)$  as a function of  $n_D$  according to Eqs. 6

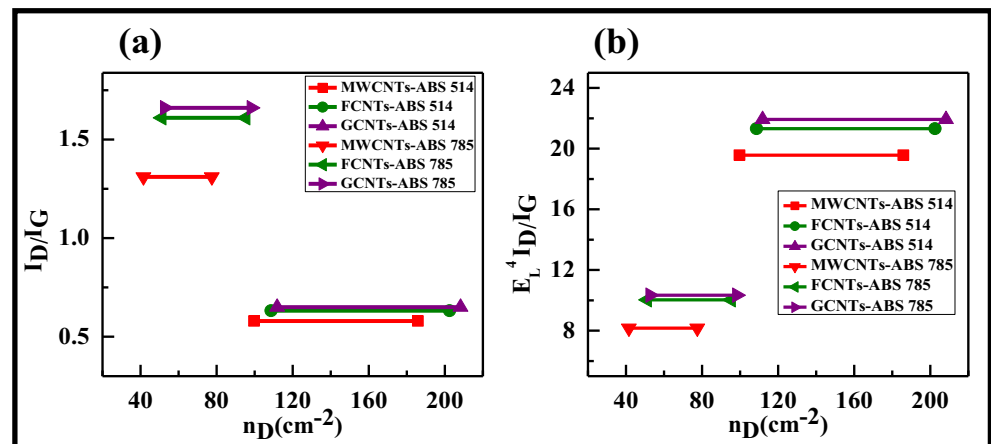
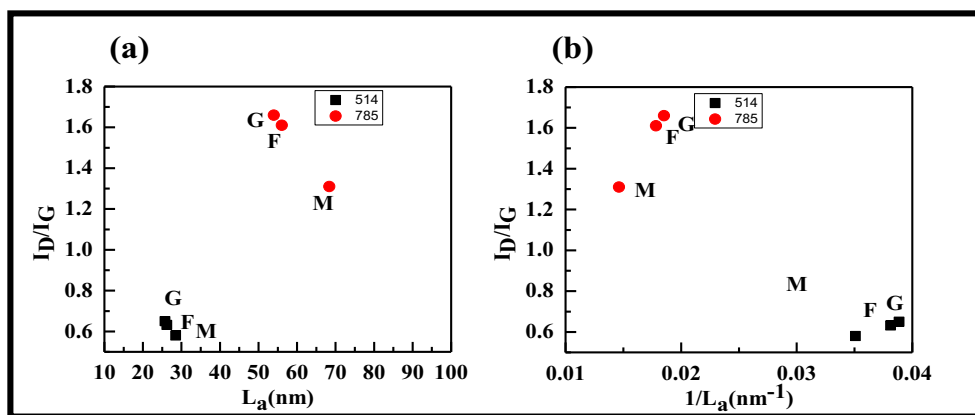


**Fig. 13** Variations of (a)  $I_D/I_G$  as function of  $L_a$  (nm) for different carbon based nanofiller reinforced ABS composites and laser excitation energy and (b)  $(I_D/I_G)$  as a function of  $1/L_a$  ( $\text{nm}^{-1}$ ) according to Eqs. 8

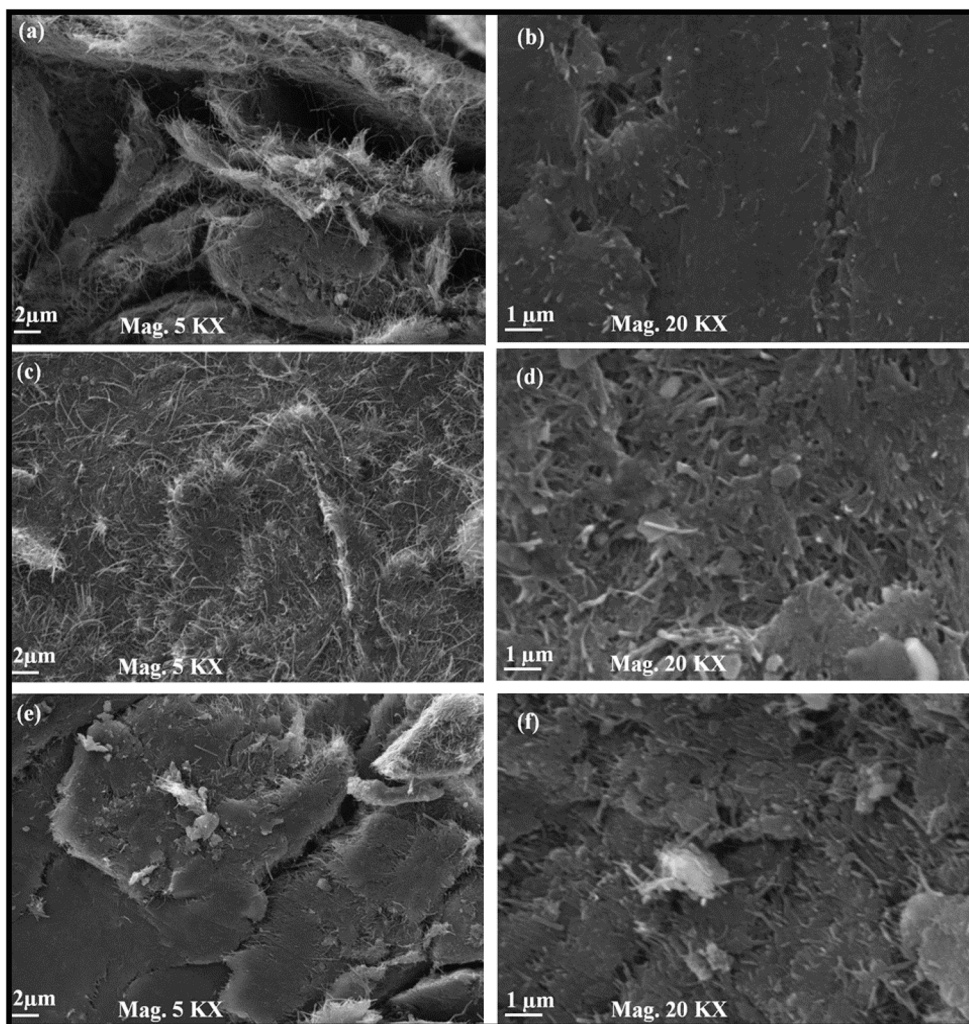


quality between the ABS and GCNTs BP enhanced the interfacial adhesion. GCNTs (Fig. 14e) showed good interaction with polymer because of the large surface area and strong bonding between GO and MWCNTs due to the presence of synergetic effect between them. Small pore dimension in BP and the high viscosity of the polymer prevent complete tube wetting, leading to a low degree of composite porosity.

**Electrical conductivity**

Generally, ABS polymer is insulating in nature and its electrical conductivity is  $10^{-12}$  S/cm [68]. Addition of the CNTs based nanofillers in the ABS matrix increased the value of electrical conductivity as shown in Fig. 15. To understand this behavior, the mechanism of electrical

**Fig. 14** SEM micrographs of (a) and (b) MWCNTs-ABS, (c) and (d) FCNTs-ABS, (e) and (f) GCNTs-ABS composites at different magnifications



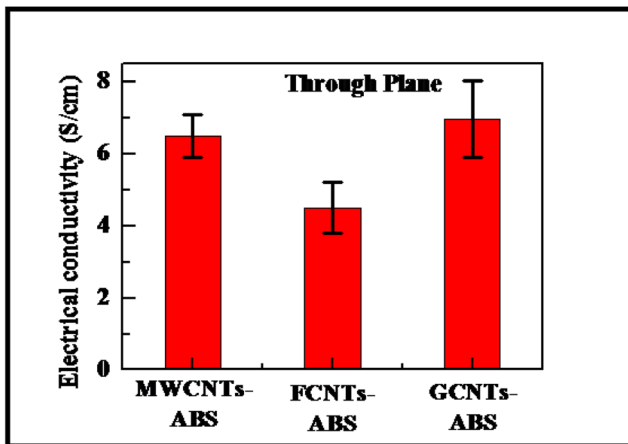


Fig. 15 Through plane DC electrical conductivity of different ABS composites

conduction within carbon based ABS composites is considered. According to the variable-range hopping (VRH) theory, [69] the electrical conduction occurs between tube–tube within a bundle or between neighbor bundles from side to side their contacts.

Generally, conductivity depends upon the two major factors, the conductivity of the nanotubes themselves and the ability to electric carriers between adjacent nanotubes. In acid treatment, some defects on the CNTs sidewalls due to functional groups which modified the conjugation system for electron transport, resulting in a slight decrement in electrical conductivity [70]. However, due to the acid treatment length of CNTs was shortened which resulted into the slightly lower electrical conductivity of FCNTs-ABS composites compared to MWCNTs-ABS composites (Fig. 15). Through plane electrical conductivity of GCNTs-ABS composites was high as compare to MWCNTs-ABS and FCNTs-ABS, because the GO sheets are attached with MWCNTs which makes the network easily in the polymer matrix and the synergistic effect of GO and CNT into GCNTs. The values of through plane electrical conductivities of MWCNTs, FCNTs and GCNTs reinforced ABS were  $6.5 \pm 0.6$ ,  $4.5 \pm 0.7$  and  $6.97 \pm 1.2$  S/cm respectively.

After the electrical conductivity, the effect of nano filler on thermal conductivity of polymer composites is studied. It depends upon the several factors like atomic size, tube size, sheet size, orientation of sheet, defect, etc.

### Thermal conductivity

Total value of the thermal conductivity is the sum of the thermal conductivity of electron and the thermal conductivity of phonon. The Wiedemann–Franz law is the ratio of the electronic contribution of the ( $\kappa$ ) to the electrical conductivity ( $\sigma$ ) of a material and is

proportional to the temperature ( $T$ ). The phonon contribution is calculated by the following equation.

$$\frac{L}{\sigma} = \kappa T \quad (10)$$

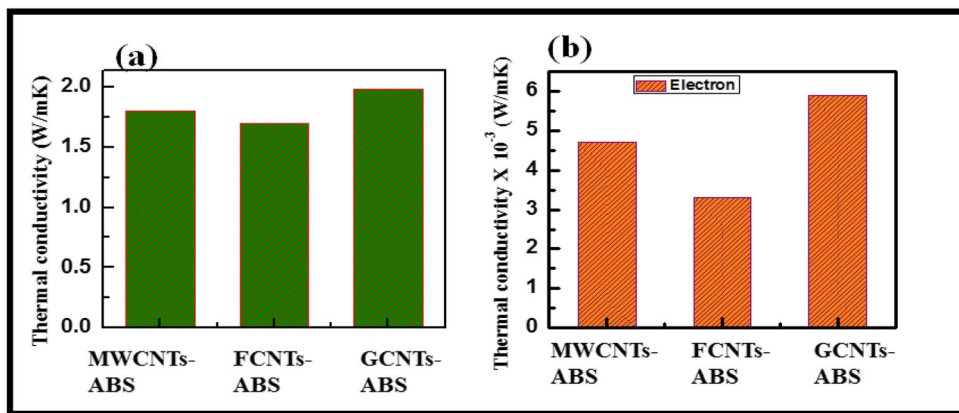
Theoretically, the proportionality constant  $L$ , known as the Lorenz number, is equal to

$$L = \frac{\kappa}{\sigma T} = \frac{\pi^2}{3} \left( \frac{\kappa_B}{e} \right)^2 = 2.44 \times 10^{-8} \text{ W}\Omega\text{K}^{-2} \quad (11)$$

Figure 16 shows the thermal conductivity ( $\kappa$ ) at room temperature for the MWCNTs-ABS, GCNTs-ABS and FCNTs-ABS composites. The values of total thermal conductivity for MWCNTs, FCNTs and GCNTs reinforced ABS composites are 1.80, 1.70 and 1.98 W/mK respectively. In the polymer composites thermal energy is mainly due to the phonon and the phonon contribution of the thermal conductivity of MWCNTs-ABS, FCNTs-ABS and GCNTs-ABS composites are large and contribution due to electron is negligible.

The application and analysis of carbon based ABS composite for the thermal transport has been investigated extensively because of the phonon domination in ballistic heat transport mechanism. The thermal conductivity is strongly depending on the degree of the entanglement, defects and chirality. The better performance of GCNTs-ABS composites is due to their specific surface and synergetic effect, as compared with FCNTs, and to the presence of the internal layers which permit phonon conduction and reducing the coupling losses. Thermal conductivity of nano composites is sensitive due to interfacial bonding between the filler and the matrix, intimately related to a phonon coupling mechanism. This mechanism is influenced by numerous factors such as the length of free path for phonons, the boundary surface scattering, the number of vibration modes, and the resistance to heat flow at the interface, known as Kapitza resistance [71]. In general, the Kapitza resistance increases with the specific surface area, decreasing the efficiency of phonon transport. GCNTs hybrid form the 3D network structure exhibits the promising potential in thermal interface due to a continuous network structure and exhibits the high value of thermal conductivity. Previous researchers showed that [72, 73] CNTs between the adjacent layers of graphene can act as additive to heat flux path and improve the thermal conductivity. The functionalization of CNTs improves the CNTs matrix interfacial bonding, thus reducing the phonon scattering between the two phase (as shown in Scheme 1) and lowered the value of thermal conductivity due to increase the defect concentration [74]. A clear demonstration of the thermal conductivity mechanism as discussed above is given in Scheme 1.

**Fig. 16** (a) Room temperature total thermal conductivity and (b) thermal conductivity due to electron contribution of MWCNTs-ABS, FCNTs-ABS and GCNTs-ABS composites

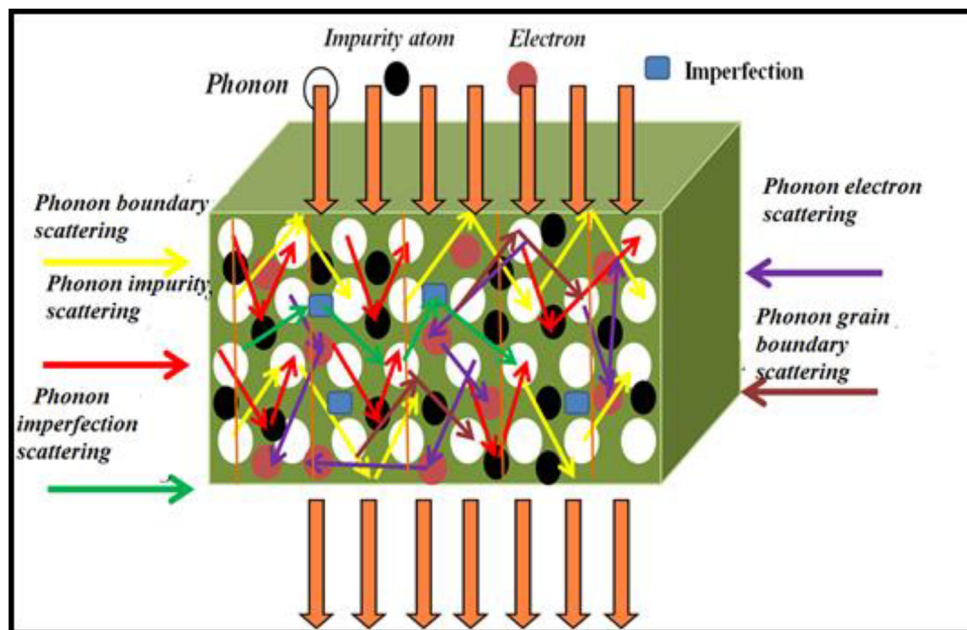


**Conclusion**

MWCNTs, FCNTs and GCNTs reinforced ABS polymer nanocomposites were prepared using vacuum filtration followed by hot compression molding. The degree of morphology, Raman, nanomechanical, electrical and thermal properties of ABS-based nanocomposites reinforced with pristine or functionalized FCNT or GCNT buckypapers were investigated. The experimental results showed that the nanomechanical properties of GCNTs-ABS were improved as compare to MWCNTs-ABS, FCNTs-ABS. The overall improvement in hardness and elastic modulus of 56.62%, 23.02% and 36.99% respectively and 70.22%, 35.52%, and 46.49%, respectively were observed for GCNTs-ABS, MWCNTs-ABS, and FCNTs-ABS over the pure ABS in nanoindentation tests. The maximum value of nanoindentation hardness and elastic modulus were 389.98±91.79 MPa and 7669.61±1179.12 MPa for GCNTs-ABS composite

respectively as compared to 248.99±26.32 MPa and 4505.7 ±261.96 MPa, respectively of pure ABS. Addition of GCNTs hybrid into ABS matrix not only reduced the deformation energy but also improved the other mechanical parameters. The enhancement in nanomechanical properties was further confirmed by Raman spectroscopic and SEM studies which exposed by the significant shifting in Raman peaks. Raman spectra of the composites with acid functionalized group of CNTs and GCNTs hybrid, ABS polymer matrix showed the noticeable shift in G and D band. MWCNTs and MWCNTs-ABS composites have higher value of  $L_D$  (21.56–12.88 (MWCNTs-514), 16.89–12.3 (MWCNTs-ABS 514)),  $L_a$  (46.4 (MWCNTs-514), 28.5 (MWCNTs-ABS 514)) and lowered value of  $n_D$  (114.07–61.24 (MWCNTs-514), 185.85–99.73 (MWCNTs-ABS 514)), due to higher purity. GCNTs and GCNTs- ABS composites have lower value of  $L_D$  (13.39–9.80 (GCNTs-514), 16–11.6 (GCNTs-ABS 514)),  $L_a$  (25.73 (GCNTs-514), 17.9 (GCNTs-ABS 514)) and higher

**Scheme 1** Schematic presentation possible in thermal diffusivity in the carbon based polymer composites



value of  $n_D$  297.36–159.63 (GCNTs-514), 208.3–111.81 (GCNTs-ABS 514)), due to defects.

The experimental values regarding electrical and thermal properties of GCNTs-ABS composites were improved as compared to MWCNTs, FCNTs reinforced ABS composites. The values of the electrical conductivity were  $6.5 \pm 0.6$ ,  $4.5 \pm 0.7$  and  $6.97 \pm 1.2$  S/cm of MWCNTs-ABS, FCNTs-ABS and GCNTs-ABS composites, respectively. The thermal conductivities values observed in MWCNTs, FCNTs and GCNTs reinforced ABS composites were 1.80, 1.70 and 1.98 W/mK, respectively. The surface morphology of the synthesized nanofiller (MWCNTs, FCNTs and GCNTs) were characterized by SEM. Due to its excellent properties, GCNTs nanofiller is a suitable material for various applications such as actuators, fuel cell catalyst supports, electrodes in supercapacitors, field emitters transistors, nanoscale generators, hydrogen gas storage, solar cells, Li-ion batteries, heat sink etc.

**Acknowledgements** The authors wish to express their gratitude to DNPL to accord the permission to publish the results. The authors would like to thank Dr. M. Saravanan for thermal conductivity measurement and Mr. J. C Ghawana for their support in preparation of samples in hydraulic press. Authors are also thankful to Mr. Jay Tawale for SEM measurement. One of the author (Jeevan Jyoti) thanks to UGC-JRF for the fellowship.

## References

- Maitra U, Prasad KE, Ramamurty U, Rao CNR (2009) Mechanical properties of nanodiamond-reinforced polymer-matrix composites. *Solid State Commun* 149(39):1693–1697
- Raghunath S, Kumar S, Samal SK, Mohanty S, Nayak SK (2018) PLA/ESO/MWCNT nanocomposite: a study on mechanical, thermal and electroactive shape memory properties. *J Polym Res* 25(5): 126
- Kong Q, Luo Z, Wang Y, Wang B (2018) Fabrication of super-stretchable and electrical conductive membrane of spandex/multi-wall carbon nanotube/reduced graphene oxide composite. *J Polym Res* 25(11):231
- Palacios JA, Ganesan R (2019) Enhancement of stiffness and dynamic mechanical properties of polymers using single-walled-carbon-nanotube—a multiscale finite element formulation study. *J Polym Res* 26(5):124
- Rafiee R, Eskandariyun A (2020) Predicting Young's modulus of agglomerated graphene/polymer using multi-scale modeling. *Compos Struct* 245:112324
- Fu X, Ramos M, al-Jumaily AM, Meshkinzar A, Huang X (2019) Stretchable strain sensor facilely fabricated based on multi-wall carbon nanotube composites with excellent performance. *J Mater Sci* 54(3):2170–2180
- Ajayan PM, Zhou OZ (2001) Applications of carbon nanotubes. In *Carbon nanotubes*. Springer. p. 391–425
- Liu Y, Kumar S (2014) Polymer/carbon nanotube nano composite fibers—a review. *ACS Appl Mater Interfaces* 6(9):6069–6087
- Esmaili A, Sbarufatti C, Jiménez-Suárez A, Ureña A, Hamouda AMS (2020) A comparative study of the incorporation effect of SWCNT-OH and DWCNT with varied microstructural defects on tensile and impact strengths of epoxy based nanocomposite. *J Polym Res* 27:152
- Mathur RB, Singh BP, Pande S (2017) Carbon nanomaterials synthesis, structure, properties and applications
- Kadambi SB, Pramoda K, Ramamurty U, Rao CNR (2015) Carbon-Nanohorn-reinforced polymer matrix composites: synergistic benefits in mechanical properties. *ACS Appl Mater Interfaces* 7(31):17016–17022
- Babal AS, Singh BP, Jyoti J, Sharma S, Arya AK, Dhakate SR (2016) Synergistic effect on static and dynamic mechanical properties of carbon fiber-multiwalled carbon nanotube hybrid polycarbonate composites. *RSC Adv* 6(72):67954–67967
- Jindal P, Jyoti J, Kumar N (2016) Mechanical characterisation of ABS/MWCNT composites under static and dynamic loading conditions. *J Mech Eng Sci* 10(3):2288–2299
- Garg P, Singh BP, Kumar G, Gupta T, Pandey I, Seth RK, Tandon RP, Mathur RB (2011) Effect of dispersion conditions on the mechanical properties of multi-walled carbon nanotubes based epoxy resin composites. *J Polym Res* 18(6):1397–1407
- Sharma S (2019) Improved static and dynamic mechanical properties of multiscale bucky paper interleaved Kevlar fiber composites. *Carbon* 152:631–642
- Sharma S, Pathak AK, Singh VN, Teotia S, Dhakate SR, Singh BP (2018) Excellent mechanical properties of long length multiwalled carbon nanotube bridged Kevlar fabric. *Carbon* 137:104–117
- Babal A et al (2014) Mechanical and electrical properties of high performance MWCNT/polycarbonate composites prepared by industrial viable twin screw extruder with Back Flow Channel. *RSC Adv* 4(110):64649–64658
- Jyoti J, Babal AS, Sharma S, Dhakate SR, Singh BP (2018) Significant improvement in static and dynamic mechanical properties of graphene oxide–carbon nanotube acrylonitrile butadiene styrene hybrid composites. *J Mater Sci* 53(4):2520–2536
- Shi Y-D, Li J, Tan YJ, Chen YF, Wang M (2019) Percolation behavior of electromagnetic interference shielding in polymer/multi-walled carbon nanotube nanocomposites. *Compos Sci Technol* 170:70–76
- Alexandre M, Dubois P (2000) Polymer-layered silicate nanocomposites: preparation, properties and uses of a new class of materials. *Mater Sci Eng R Rep* 28(1):1–63
- Jyoti J, Basu S, Singh BP, Dhakate SR (2015) Superior mechanical and electrical properties of multiwall carbon nanotube reinforced acrylonitrile butadiene styrene high performance composites. *Compos Part B* 83:58–65
- Kumar A, Sharma K, Dixit AR (2020) Carbon nanotube-and graphene-reinforced multiphase polymeric composites: review on their properties and applications. *J Mater Sci*, 1–43
- Zhang Y et al (2005) Experimental observation of the quantum Hall effect and Berry's phase in graphene. *Nature* 438(7065):201–204
- Lee C, Wei X, Kysar JW, Hone J (2008) Measurement of the elastic properties and intrinsic strength of monolayer graphene. *Science* 321(5887):385–388
- Balandin AA (2011) Thermal properties of graphene and nanostructured carbon materials. *Nat Mater* 10(8):569–581
- Park S, Ruoff RS (2009) Chemical methods for the production of graphenes. *Nat Nanotechnol* 4(4):217–224
- Alsharaeh EH, Faisal NH, Othman AA, Ahmed R (2013) Evaluation of nanomechanical properties of (styrene–methyl methacrylate) copolymer composites containing graphene sheets. *Ind Eng Chem Res* 52(50):17871–17881
- Jyoti J, Singh BP, Chockalingam S, Joshi AG, Gupta TK, Dhakate SR (2018) Synergistic effect of graphene oxide-carbon nanotube on

- nanomechanical properties of acrylonitrile butadiene styrene nanocomposites. *Mater Res Express* 5(4):045608
29. Ramanathan T, Abdala AA, Stankovich S, Dikin DA, Herrera-Alonso M, Piner RD, Adamson DH, Schniepp HC, Chen X, Ruoff RS, Nguyen ST, Aksay IA, Prud'Homme RK, Brinson LC (2008) Functionalized graphene sheets for polymer nanocomposites. *Nat Nanotechnol* 3(6):327–331
  30. Wang H, Hao Q, Yang X, Lu L, Wang X (2010) A nanostructured graphene/polyaniline hybrid material for supercapacitors. *Nanoscale* 2(10):2164–2170
  31. Choi BG, Yang MH, Hong WH, Choi JW, Huh YS (2012) 3D macroporous graphene frameworks for supercapacitors with high energy and power densities. *ACS Nano* 6(5):4020–4028
  32. Berger C, Song Z, Li T, Li X, Ogbazghi AY, Feng R, Dai Z, Marchenkov AN, Conrad EH, First PN, de Heer WA (2004) Ultrathin epitaxial graphite: 2D electron gas properties and a route toward graphene-based nanoelectronics. *J Phys Chem B* 108(52):19912–19916
  33. Gwon H, Kim HS, Lee KU, Seo DH, Park YC, Lee YS, Ahn BT, Kang K (2011) Flexible energy storage devices based on graphene paper. *Energy Environ Sci* 4(4):1277–1283
  34. Li N, Zheng M, Lu H, Hu Z, Shen C, Chang X, Ji G, Cao J, Shi Y (2012) High-rate lithium–sulfur batteries promoted by reduced graphene oxide coating. *Chem Commun* 48(34):4106–4108
  35. Jyoti J, Singh BP, Rajput S, Singh VN, Dhakate SR (2016) Detailed dynamic rheological studies of multiwall carbon nanotube-reinforced acrylonitrile butadiene styrene composite. *J Mater Sci* 51(5):2643–2652
  36. Jyoti J, Kumar A, Dhakate SR, Singh BP (2018) Dielectric and impedance properties of three dimension graphene oxide-carbon nanotube acrylonitrile butadiene styrene hybrid composites. *Polym Test* 68:456–466
  37. Jyoti J, Dhakate SR, Singh BP (2018) Phase transition and anomalous rheological properties of graphene oxide-carbon nanotube acrylonitrile butadiene styrene hybrid composites. *Compos Part B* 154:337–350
  38. Wang Z, Cao Y, Pan D, Hu S (2020) Vertically aligned and interconnected graphite and Graphene oxide networks leading to enhanced thermal conductivity of polymer composites. *Polymers* 12(5):1121
  39. Zhang C, Tjiu WW, Liu T, Lui WY, Phang IY, Zhang WD (2011) Dramatically enhanced mechanical performance of nylon-6 magnetic composites with nanostructured hybrid one-dimensional carbon nanotube–two-dimensional clay nanoplatelet heterostructures. *J Phys Chem B* 115(13):3392–3399
  40. Zhang WD, Phang IY, Liu T (2006) Growth of carbon nanotubes on clay: unique nanostructured filler for high-performance polymer Nanocomposites. *Adv Mater* 18(1):73–77
  41. Dubois P, Alexandre M (2006) Performant clay/carbon nanotube polymer nanocomposites. *Adv Eng Mater* 8(3):147–154
  42. Zhang Q, Zhao M, Liu Y, Cao A, Qian W, Lu Y, Wei F (2009) Energy-absorbing hybrid composites based on alternate carbon-nanotube and inorganic layers. *Adv Mater* 21(28):2876–2880
  43. Sun D, Chu C-C, Sue H-J (2010) Simple approach for preparation of epoxy hybrid nanocomposites based on carbon nanotubes and a model clay. *Chem Mater* 22(12):3773–3778
  44. Kapoor S, Goyal M, Jindal P (2020) Effect of functionalized multi-walled carbon nanotubes on thermal and mechanical properties of acrylonitrile butadiene styrene nanocomposite. *J Polym Res* 27(2): 40
  45. Kavimani V, Soorya Prakash K, Thankachan T, Udayakumar R (2020) Synergistic improvement of epoxy derived polymer composites reinforced with Graphene Oxide (GO) plus Titanium di oxide (TiO<sub>2</sub>). *Compos Part B* 191:107911
  46. Zhao MQ, Zhang Q, Jia XL, Huang JQ, Zhang YH, Wei F (2010) Hierarchical composites of single/double-walled carbon nanotubes interlinked flakes from direct carbon deposition on layered double hydroxides. *Adv Funct Mater* 20(4):677–685
  47. Shin MK, Lee B, Kim SH, Lee JA, Spinks GM, Gambhir S, Wallace GG, Kozlov ME, Baughman RH, Kim SJ (2012) Synergistic toughening of composite fibres by self-alignment of reduced graphene oxide and carbon nanotubes. *Nat Commun* 3:650
  48. Chatterjee S, Nafezarefi F, Tai NH, Schlagenhaut L, Nüesch FA, Chu BTT (2012) Size and synergy effects of nanofiller hybrids including graphene nanoplatelets and carbon nanotubes in mechanical properties of epoxy composites. *Carbon* 50(15):5380–5386
  49. Gong S et al. (2015) Integrated ternary bioinspired Nanocomposites via synergistic toughening of reduced Graphene oxide and double-walled carbon nanotubes. *ACS Nano*
  50. Kim NH, Kuila T, Lee JH (2014) Enhanced mechanical properties of a multiwall carbon nanotube attached pre-stitched graphene oxide filled linear low density polyethylene composite. *J Mater Chem A* 2(8):2681–2689
  51. Yang Y, He CE, Tang W, Tsui CP, Shi D, Sun Z, Jiang T, Xie X (2014) Judicious selection of bifunctional molecules to chemically modify graphene for improving nanomechanical and thermal properties of polymer composites. *J Mater Chem A* 2(47):20038–20047
  52. Fan Z, Wang J, Wang Z, Ran H, Li Y, Niu L, Gong P, Liu B, Yang S (2014) One-pot synthesis of graphene/hydroxyapatite nanorod composite for tissue engineering. *Carbon* 66:407–416
  53. Mathur R, Chatterjee S, Singh B (2008) Growth of carbon nanotubes on carbon fibre substrates to produce hybrid/phenolic composites with improved mechanical properties. *Compos Sci Technol* 68(7–8):1608–1615
  54. Singh BP et al (2014) Effect of length of carbon nanotubes on electromagnetic interference shielding and mechanical properties of their reinforced epoxy composites. *J Nanopart Res* 16(1):1–11
  55. Singh B et al (2008) Influence of surface modified MWCNTs on the mechanical, electrical and thermal properties of polyimide nanocomposites. *Nanoscale Res Lett* 3(11):444–453
  56. Marcano DC, Kosynkin DV, Berlin JM, Sinitskii A, Sun Z, Slesarev A, Alemany LB, Lu W, Tour JM (2010) Improved synthesis of graphene oxide. *ACS Nano* 4(8):4806–4814
  57. Dwivedi N, Kumar S, Malik HK (2011) Nanoindentation measurements on modified diamond-like carbon thin films. *Appl Surf Sci* 257(23):9953–9959
  58. Ram HA, Koppad PG, Kashyap K (2013) Nanoindentation studies on MWCNT/aluminum alloy 6061 nanocomposites. *Mater Sci Eng A* 559:920–923
  59. Ostovan F, Matori K, Toozandehjani M, Oskoueian A, Yusoff H, Yunus R, Mohamed Ariff A (2016) Nanomechanical behavior of multi-walled carbon nanotubes particulate reinforced aluminum Nanocomposites prepared by ball milling. *Materials* 9(3):140
  60. Oliver WC, Pharr GM (1992) An improved technique for determining hardness and elastic modulus using load and displacement sensing indentation experiments. *J Mater Res* 7(06):1564–1583
  61. Dwivedi N, Kumar S, Rauthan CMS, Panwar OS (2011) Nano indentation measurements on nitrogen incorporated diamond-like carbon coatings. *Applied Physics A* 102(1):225–230
  62. Díez-Pascual AM, Naffakh M, Gómez MA, Marco C, Ellis G, Martínez MT, Ansón A, González-Domínguez JM, Martínez-Rubi Y, Simard B (2009) Development and characterization of PEEK/carbon nanotube composites. *Carbon* 47(13):3079–3090
  63. Dresselhaus MS, Dresselhaus G, Saito R, Jorio A (2005) Raman spectroscopy of carbon nanotubes. *Phys Rep* 409(2):47–99
  64. Papageorgiou DG, Kinloch IA, Young RJ (2017) Mechanical properties of graphene and graphene-based nanocomposites. *Prog Mater Sci* 90:75–127
  65. Lucchese MM, Stavale F, Ferreira EHM, Vilani C, Moutinho MVO, Capaz RB, Achete CA, Jorio A (2010) Quantifying ion-induced defects and Raman relaxation length in graphene. *Carbon* 48(5):1592–1597

66. Cançado LG, Jorio A, Ferreira EHM, Stavale F, Achete CA, Capaz RB, Moutinho MVO, Lombardo A, Kulmala TS, Ferrari AC (2011) Quantifying defects in graphene via Raman spectroscopy at different excitation energies. *Nano Lett* 11(8):3190–3196
67. Cancado L et al (2006) General equation for the determination of the crystallite size  $L_a$  of nanographite by Raman spectroscopy. *Appl Phys Lett* 88(16):163106–163106
68. Shrivastava N et al. (2014) Influence of selective dispersion of MWCNT on electrical percolation of in-situ polymerized high-impact polystyrene/MWCNT nanocomposites. *Express Polym Lett* 8(1)
69. Mott NF, Davis EA (2012) *Electronic processes in non-crystalline materials*. Oxford University Press, Oxford
70. Jackson R, Domercq B, Jain R, Kippelen B, Graham S (2008) Stability of doped transparent carbon nanotube electrodes. *Adv Funct Mater* 18(17):2548–2554
71. Kapitza P (1941) The study of heat transfer in helium II. *J Phys (USSR)* 4(1–6):181–210
72. Warzoha RJ, Zhang D, Feng G, Fleischer AS (2013) Engineering interfaces in carbon nanostructured mats for the creation of energy efficient thermal interface materials. *Carbon* 61:441–457
73. Feng W, Qin M, Lv P, Li J, Feng Y (2014) A three-dimensional nanostructure of graphite intercalated by carbon nanotubes with high cross-plane thermal conductivity and bending strength. *Carbon* 77:1054–1064
74. Yu A, Itkis ME, Bekyarova E, Haddon RC (2006) Effect of single-walled carbon nanotube purity on the thermal conductivity of carbon nanotube-based composites. *Appl Phys Lett* 89(13):133102

**Publisher's note** Springer Nature remains neutral with regard to jurisdictional claims in published maps and institutional affiliations.